

# An HST Archival Survey of Feathers in Spiral Galaxies

Misty A. La Vigne, Stuart N. Vogel, and Eve C. Ostriker

*Department of Astronomy, University of Maryland, College Park, MD 20742*

## ABSTRACT

We present a survey of spiral arm extinction substructure referred to as feathers in 223 spiral galaxies using HST WFPC2 images. The sample includes all galaxies in the RC3 catalog with  $cz < 5000 \text{ km s}^{-1}$ ,  $B_T < 15$ ,  $i < 60^\circ$ , and types Sa–Sd with well-exposed broadband WFPC2 images. The detection frequency of delineated, periodic feathers in this sample is 20% (45 of 223). This work is consistent with Lynds (1970), who concluded that feathers are common in prototypical Sc galaxies; we find that feathers are equally common in Sb galaxies. Sb–Sc galaxies without clear evidence for feathers either had poorer quality images, or flocculent or complex structure. We did not find clearly defined feathers in any Scd–Sd galaxy. The probability of detecting feathers was highest (83%) for spirals with well-defined primary dust lanes (the lanes which line the inner edge of an arm); well-defined primary dust lanes were only noted in Sab–Sc galaxies. The detection frequency of feathers was similar in barred and unbarred spirals. Consistent with earlier work, we find that neighboring feathers tend to have similar shapes and pitch angles. Well-defined feathers often emerge from the primary dust lane as leading features before they curve to trailing; some are quite elongated, extending into the interarm and merging with other feathers. OB associations are often found lining feathers, and many feathers transition to the stellar substructures known as spurs (Elmegreen 1980). We find that feathers are coincident with interarm filaments strikingly revealed in Spitzer  $8\mu\text{m}$  images. Comparison with CO 1-0 maps of NGC 0628 and NGC 5194 from BIMA SONG shows that feathers originate at the primary dust lane coincident with gas surface density peaks. Contrary to the appearance at  $8\mu\text{m}$ , the CO maps show that gas surface density in feathers decreases rapidly with distance from the primary dust lane. Also, we find that the spacing between feathers decreases with increasing gas surface density; consistent with formation via a gravitational instability.

*Subject headings:* galaxies: ISM — galaxies: spiral — surveys — galaxies: structure

## 1. Introduction

Spiral arms are not smooth, continuous features. Typically an arm is composed of many substructures commonly referred to as feathers, spurs, and branches, which give the arm its patchy, divaricate appearance. This substructure appears associated with much of the star formation in the arm.

### 1.1. Previous Observations of Spiral Arm Substructure

Early reports of spiral arm substructure were based on examination of photographic plates such as those used for prints in *The Hubble Atlas of Galaxies* (Sandage 1961). Weaver (1970) noted that the spiral arms of nearby galaxies appear clumpy, irregular, and mottled on small scales. In particular, he noted the presence of “spurs” (also referred to as branches or twigs), which appear to originate on the *outside* of the arm, with larger pitch angles than the arm itself. Spurs extend from the outside of the arm into the interarm, and are seen in photographic plates as *stellar* features. Weaver also noted the presence of *dark* material concentrated along the *inner* edges of spiral arms. He remarked that the outside regions of arms appear to be made of material drawn out or “brushed” from the inner edges, and that this brushed-out structure has a pitch angle typically a factor of two larger than the arm itself.

At the same time, Lynds (1970) reported a detailed study of dark nebulae in 17 late-type spirals using photographic plates from Mt. Wilson and Palomar Observatories. She commented on the well-known strong dust lanes along the inner edge of the arms, which she termed “primary dust lanes” (hereafter abbreviated PDLs), and noted the presence of thin dust lanes with large pitch angles cutting *across* the luminous arms. She called these features “feathers”, and pointed out that these extinction features become mostly undetectable outside the luminous arm presumably owing to the absence of a sufficiently bright background. She also emphasized that bright HII regions are typically near or embedded in dust lanes. Later, Piddington (1973) noted that interarm stellar features called spurs by Weaver are often found associated with the extinction features cutting across luminous arms called feathers by Lynds, and suggested that the two are related.

Subsequently, Elmegreen (1980) studied seven spiral galaxies to investigate the properties of spurs, which as noted above are observable as stellar features. Elmegreen was able to identify two to six well-delineated spurs in each of her galaxies, with lengths ranging from one to five kpc; her spurs are generally located in the outer parts of the luminous disk. She observed that spurs are always located on the outside of spiral arms, have pitch angles equal

to or greater than that of the originating arm, and commonly occur in pairs or groups with the spurs oriented roughly parallel to one another. Elmegreen also determined that on average spurs have pitch angles of roughly  $50^\circ$  with respect to spiral arms, which is comparable to the average pitch angles of the feathers measured by Lynds (1970). Noting the similarity between the pitch angles of feathers and spurs, Elmegreen added further observational support to Piddington’s (1973) suggestion that spurs and feathers have a common origin.

## 1.2. Theoretical Studies of Substructure

Motivated to explain the formation of observed spurs, branches, and feathers in spiral galaxies, Balbus (1988, hereafter B88) conducted a local gas dynamical stability analysis of a single-fluid polytropic flow through spiral arm potentials, following the linear evolution of self-gravitating perturbations. In his analysis, the background gaseous surface density profile representing the arm has an arbitrary spatial form, and the differentially rotating, expanding background flow is consistent with this profile. Balbus investigated all wavenumber directions in the plane of the disk and modeled the spiral arms as tightly wound, with no magnetic field. B88 found that there are two preferred directions of growth in spiral arm flow: initial wavefronts roughly along the spiral arm, or perpendicular to it. The rate of growth in both directions depends on the properties of the underlying flow. In certain regimes, growth of instabilities leads to fragmentation parallel to the arms, observed as a thickening of the arms. In other situations, growth of initially leading wavenumbers results in branches, feathers, or spurs. For wavefronts initially perpendicular to the arm, as the gas moves into the interarm region, the flow expansion and shear (which increases downstream from the arm) shapes and stretches small-scale structure into the familiar large scale trailing ‘spur’ shapes that are observed.

B88 also suggested that a two-dimensional lattice of small-scale structure can develop when the two dominant modes of growth intersect. In *The Hubble Atlas of Galaxies* (Sandage 1961), B88 found that some barred spiral galaxies, in particular the western arm of NGC 1300, seemed to exhibit a lattice structure of HII regions. However, he found no examples of such structure in unbarred galaxies.

Kim and Ostriker (2002, hereafter KO) extended the local models of B88 by including the effects of non-linearity and magnetic fields. KO conducted local, two-dimensional, time-dependent, magneto-hydrodynamic (MHD) simulations of self-gravitating, differentially rotating, razor thin disks of gas. Their models followed the formation and fragmentation of “gaseous spurs” as the flow passes through spiral arm potentials. They found that local substructures are created via the magneto-Jeans instability (MJI); as the background flow

passes through the spiral pattern it is shocked and compressed until it becomes Jeans unstable, at which point gravity, aided by magnetic forces, begins to create alternating compressed and rarefied regions along an arm. The magnetic effects aid the formation of compressed, self-gravitating complexes because magnetic tension forces oppose the Coriolis forces that would otherwise stabilize the flow, helping to transfer angular momentum out of growing condensations. KO found that the gaseous spurs fragment into clumps within which star formation could commence. They suggest that these clumps could be the precursors of bright HII regions that jut from the outside of spiral arms inside corotation.

From their simulations, KO put together observable statistics of their gaseous spurs. Most potentially comparable to observations is the spacing of these features along a spiral arm, which they find ranges from 2–5 times the local Jeans wavelength (at the spiral arm density peak) and corresponds to a spacing of approximately 750 pc on average. KO also proposed that the shape and location of gaseous spurs within a spiral arm may potentially be used observationally to determine the spiral pattern speed of the arm. Very recently, Kim & Ostriker (2006) have extended their thin disk simulations to three dimensions, also making comparison to two-dimensional “thick disk” models. The results they find are overall consistent with the conclusions of KO, with the difference that spur spacings increase by a factor  $\sim 2$  due to the dilution of self gravity when the disk thickness increases.

Chakrabarti, Laughlin, and Shu (2003, hereafter CLS) studied the response of a thin, self-gravitating, singular isothermal gaseous disk to rigidly rotating spiral potentials, specifically focusing on the effects of ultraharmonic resonances by choosing parameters that minimize swing amplification. In simulations with low  $Q_g$ , CLS found growth of spiral arm “branches” (which they define as trailing bifurcations of the main spiral arms). Long-term simulations with high  $Q_g$  exhibited the growth of stubby leading structures (referred to as “spurs” by CLS; this is however inconsistent with terminology of other authors).

Wada and Koda (2004, hereafter WK) performed two-dimensional, time dependent, global hydrodynamical simulations of a thin, isothermal, non-self-gravitating disk of gas in tightly and loosely wound, rigidly rotating spiral potentials. WK’s model rotation profiles included both differentially rotating and rigidly rotating cases. They found that the spiral shock front is stable when the gas is modeled with a flat rotation curve and unstable when modeled with a rising rotation curve. In their models, they found the stability of the shock front is also dependent upon the pitch angle of the spiral arms: stable if  $i \leq 10^\circ$ , unstable if  $i \geq 10^\circ$ . In the unstable models of WK, strong shocks with arm-interarm density ratio  $\sim 100$  become unstable by rippling. WK attribute this “wiggle” instability to Kelvin-Helmholtz (K-H) modes involving the strong velocity shear behind the shock. Over time, the instabilities become non-linear forming what WK refer to as “spurs” in the interarm regions. The

spurs are quasi-regularly spaced, approximately 100-200 pc apart; the authors do not state, however, how spacing depends on model parameters. Due to the shape of the rotation curve, the spurs formed in the WK simulations are curved near the arm in the opposite sense (i.e. trailing then leading) to the gaseous spurs produced in the KO simulations and the small-scale structure predicted in B88’s analysis.

Dobbs and Bonnell (2006, hereafter DB) used three-dimensional SPH simulations to study the response of isothermal, non-self-gravitating gaseous disk models with varying temperatures to a four armed rigidly-rotating spiral potential. DB find that the temperature of the disk has a crucial effect on the growth of spiral arm substructure. In the lower temperature ( $T < 10^3$  K) models of DB, the initially smooth arms become clumpy, and then the clumps are sheared into trailing features as they return to interarm regions. The shapes of the interarm features found by DB are similar to those of KO, reflecting the flat rotation curve they adopt. DB use somewhat nonstandard terminology in describing their results; they refer to the portions of interarm extinction features adjoining arms as “spurs”, and the portions further downstream as “feathers”. In their  $T = 50$  K model, which has arm-interarm contrast  $\sim 50$ , the spacing of DB’s spurs are  $\approx 700$  pc; DB also do not state, however, how spacing depends on model parameters.

### 1.3. Discussion of Substructure Nomenclature

As is evident from the above summaries, the terms “spurs”, “feathers”, and “branches” have been used in many ways. In this paper, we adopt the definitions from the initial, observational papers:

*feathers* – thin dust lanes or extinction features that extend outward at a large angle from the *primary dust lane* (PDL) which lines the inner side of the arm, cutting across the outer bright part of the spiral arm (Lynds 1970).

*spurs* – bright chains of OB associations and HII regions that jut at a large angle from the spiral arm into the interarm (Weaver 1970, Elmegreen 1980).

*branches* – divarications of a spiral arm that lend to the overall spiral structure (Elmegreen 1980).

### 1.4. A New Survey of Spiral Arm Feathers

Feathers are of considerable interest because there are both observational (Lynds 1970, Piddington 1973, Elmegreen 1980, Scoville et al. 2001) and theoretical (B88, KO) reasons to associate them with a significant portion of star formation in spiral galaxies. Also, they may provide information on basic physical conditions in spiral arms, such as the mean gaseous surface density and magnetic field strength (KO). At least in principle, they may also be used to deduce the spiral pattern speed and details of the gas flow through spiral arms (KO, CLS). Lastly, they are a striking characteristic of prototypical grand design spiral galaxies (e.g. M51, Beckwith 2005) and may therefore tell us something about the evolutionary and environmental aspects of spiral structure. A complete description of spiral arms should include a characterization of the frequency and properties of such feathers, and a complete model of spiral structure should explain their dynamical origins.

The goals of this survey include: confirming that feathers are a common feature of spiral galaxies, evaluating their frequency and characteristics, and determining the types of spiral galaxies in which feathers occur (barred or unbarred, early or late-type, grand design or flocculent). We aim to identify where feathers are located: in the inner or outer disk, on the inside of spiral arms or the outside? In addition, we investigate the relation of the spacing of feathers to the gas surface density of a galaxy.

## 2. Sample Selection

Our study was motivated by the WFPC2 Hubble Heritage image of M51 (Scoville et al. 2001), which revealed remarkable feather structure particularly in the inner galaxy. Since similar structure is difficult to discern in a casual inspection of M51 and other galaxies in *The Hubble Atlas of Galaxies* (Sandage 1961), we concluded that high angular resolution is important and sought to explore the Hubble Space Telescope (HST) archives for additional examples of galaxies with clearly delineated feathers.

The HST archive contains thousands of galaxy images. To narrow the list, we initially used the Elmegreen & Elmegreen (1987; hereafter EE) sample of 762 spirals, each classified as one of nine arm types ranging from “chaotic, fragmented, unsymmetric” to “two long symmetric arms dominating the optical disk”. The EE sample might appear ideal, since we expected galaxies with well-defined spiral arms to be the best targets. However, many galaxies classified as grand design by EE have poorly-defined arms in HST images. Conversely, many galaxies classified by EE as having poorly-defined arms have well-defined arms in HST images. The EE classifications appear to be determined primarily by the arm structure

outside the inner  $1'$  of galaxies, beyond the region typically imaged by HST. This may be because in the Palomar Sky Survey images used by EE the inner arms are often saturated and the outer arms dominate the spiral structure. We conclude that EE arm classes do not provide reliable descriptions of arm type in the inner  $1'$  of many nearby galaxies.

We therefore expanded our search using the *Third Reference Catalogue of Bright Galaxies* (RC3). This increased the sample size by including galaxies at more southern declinations not available in the EE sample, and allowed us to specify criteria optimized for identification of substructures. Based on the absence of clear examples of feathers in the photographic reproductions of ground-based images in the Hubble Atlas, we decided that distance to a galaxy should be the primary criterion for inclusion in the sample.

## 2.1. A Distance-Limited Sample

Using Vizier, we selected all galaxies in the RC3 catalog with de Vaucouleurs type Sa–Sd,  $cz < 5000 \text{ km s}^{-1}$ ,  $i < 60^\circ$ , and  $B_T < 15$ . Our sample excludes galaxies with type Sdm or later because these typically lack well-delineated spiral arms.

The recessional velocity was limited to  $< 5000 \text{ km s}^{-1}$  to ensure adequate linear resolution to resolve typical dust lanes and any substructure that may be present. Assuming  $H_o = 71 \text{ km s}^{-1} \text{ Mpc}^{-1}$ , this redshift corresponds to a linear resolution of 34 pc for the  $0.1''$  resolution of the three Wide Field Cameras. The limit for inclination was set to  $60^\circ$  because at higher inclinations a galaxy may be too inclined to clearly discern structure. The  $B_T$  magnitude was limited to galaxies brighter than 15th magnitude to eliminate small galaxies or low surface brightness galaxies, neither of which would be well suited for examination of extinction substructure. (In fact, few galaxies in the RC3 catalog at  $cz < 5000 \text{ km s}^{-1}$  have  $B_T > 15$ , so this criterion did not significantly affect the sample size.) The total number of galaxies that meet these criteria is 630.

Ideally, for detection of feathers (extinction substructure), we need images taken with high resolution, a large field of view (FOV), and good sensitivity. These criteria are best satisfied by the HST ACS (Advanced Camera for Surveys) instrument. However, many of the ACS images were still proprietary at the time of this study. We therefore used images taken with WFPC2 (Wide Field/Planetary Camera 2), which also satisfies the above criteria.

Since good signal-to-noise ratios are essential, we restricted the sample to images with exposure time  $> 60$  seconds obtained with wideband (W) filters. All images taken with filters shorter than  $4311 \text{ \AA}$  and longer than  $8012 \text{ \AA}$  were excluded due to the poor sensitivity of WFPC2 at shorter wavelengths, and because extinction features are less prominent at

longer optical wavelengths. Lastly, observations of galaxies where the FOV did not cover a spiral arm were excluded from the sample. We found that 223 of the 630 RC3 galaxies had WFPC2 images meeting our criteria.

### 3. Data Reduction

We obtained from the HST archive calibrated, full resolution FITS files for images of all 223 galaxies which met the selection criteria described above. We then mosaiked the images and removed cosmic rays using standard procedures outlined in the HST handbook.

We selected images of 21 of the galaxies with well-defined substructure to present as prototypes (see Figures 1–14). Typically the original images vary significantly in brightness between the nucleus and outer regions, making it difficult to see substructure in different parts of the galaxy in a single image stretch. Therefore, images shown in the figures were further processed by subtracting a radial profile derived from the median value in annuli deprojected assuming the RC3 inclination and using nuclear positions obtained from the NASA/IPAC Extragalactic Database (NED).

## 4. Results

### 4.1. General Characteristics of Feathers

We illustrate many of the general characteristics of classic feathers using HST observations of NGC 5194 and NGC 0628. Images are shown in Figures 1 and 2 with thin lines to mark identified feathers, and in Figures 3 and 4 without the lines. Each arm exhibits dark, delineated extinction features, which emerge from the primary dust lane (PDL) that runs along the inside part of the arm, traverse across the luminous arm, and often extend into the interarm.

Typically, close inspection shows that well-delineated feathers emerge from the PDL as leading features and then gradually curve to become trailing features further downstream, on the outer edges of the spiral arms. Feathers that are near each other generally have similar pitch angles and curvature, as noted by Lynds (1970). Many are dotted with bright knots of star formation or HII regions, especially near the PDLs and the beginning of the interarm regions.

Many of the feathers extend well into the interarm regions. Several coalesce and can be traced through more than  $180^\circ$ . The farthest-reaching feathers appear to merge with the



PDL of the next arm, as is seen in both arms of NGC 0628 and NGC 5194.

## 4.2. Frequency of Feather Detections

Motivated by the observational and theoretical studies reviewed in §1.1 and §1.2, we considered a galaxy to have well-defined, classic feathers if it exhibited extinction substructure meeting the following criteria: multiple dust lanes with approximately regular spacing emerging from a PDL at roughly similar large angles, frequently associated with star formation regions.

Feathers were clearly detected in 45 of the 223 (20%) galaxies examined. To investigate which galaxies have feathers, we classified all 223 galaxies according to how well the spiral arm PDLs are delineated, using the HST images. PDL delineation was categorized from “poor” (see NGC 5055, Figure 12) to “fair” (see NGC 1300, Figure 6) to “good” (see NGC 4548, Figure 10). Table 1 lists the number and percentage of galaxies with clear detections of feathers for each of the three PDL classifications. We see that the presence of delineated PDLs and feathers are highly correlated: 83% of galaxies with good PDL delineation show feathers. However, not all galaxies with delineated PDLs have feathers. NGC 4450 is an example of a galaxy with delineated PDLs categorized as good which has no feathers. Interestingly, NGC 4450 is also classified as an anemic galaxy (Elmegreen et al. 2002).

The feathers detected in the 45 galaxies mentioned above originate at delineated PDLs. We also find features resembling feathers present in flocculent galaxies that do not satisfy our strict definition of feathers because they do not appear to originate at a PDL (as well as in four flocculent galaxies with feathers that clearly do originate at PDLs). We detected such “flocculent feathers” in 17 out of 24 flocculent galaxies. We do not include cases of flocculent feathers without PDLs in Table 2.

Also, within the central kiloparsec of some galaxies the images reveal fine, smaller scale extinction features. These interesting features, seen for example in NGC 5194 (Figure 3), also do not appear to originate at a PDL and therefore we do not classify them as classic feathers. Occasionally, the extinction features present could be interpreted as lattice structure.

In general, from our sample of 223, those galaxies in which we did not definitively detect feathers fall into one or more of the following categories: a) the galaxy image is of lesser quality, typically due to exposure time or distance of the galaxy; b) PDLs are not clearly detected, which in some cases may be due to the quality of the observations; c) the galaxy is a flocculent with no clear PDLs; or d) the spiral arm structure is too complex or confusing, sometimes as the result of interaction.

### 4.3. Feather Frequency and Characteristics as a Function of Galaxy Type

Previous observational work emphasized that feathers and spurs are a characteristic of late-type spirals (e.g. Lynds 1970; Elmegreen 1980). Figure 17 shows that the sample of 223 spirals is sufficiently large to investigate feather frequency for all types of spirals. We see that feathers are most common in Sb–Sc galaxies, with feathers clearly detected in 26–33%.

At earlier Hubble types, the detection frequency is lower: 4/24 or 17% for Sab and 1/28 for Sa. Clearly, feathers are quite common in somewhat earlier types (e.g. Sb) than previously thought. For example, NGC 4736 (Sab) shows particularly clear feathers, as seen in Figure 11. Still, feathers are definitely rarer at the earliest types. This may be in part because some early type galaxies are relatively deficient in gas, or because the shallower pitch angle of the arms results in lower shock compression of the PDL. Both of these might result in weaker PDLs; indeed, well-defined PDLs are detected in none of the 28 Sa galaxies and only 4 of the 24 Sab galaxies, compared to 31 of 129 Sb–Sc galaxies.

At later Hubble types, there are no feathers detected (0/37 for Scd and 0/15 for Sd). Note that no well-defined PDLs are detected in the 47 Scd–Sd galaxies, presumably because the spiral density enhancement is relatively weak in these generally lower luminosity galaxies, and this likely accounts for the paucity of feathers.

We found little difference between barred and unbarred galaxies in the frequency of feather detection. In particular, the frequencies are 14/66 (21%) for SA, 17/78 (22%) for SAB, and 14/73 (19%) for SB. As will be discussed in §4.4, parallel PDLs and “lattice” feather structure connecting the parallel PDLs are common in the arms of barred spirals.

We expected feathers to be associated with grand design spirals. We were surprised to find feathers and PDLs in some flocculent spirals as well, since flocculents appear “fleecy” at optical wavelengths and typically lack large-scale, continuous spiral structure. This absence of large-scale, continuous spiral structure is generally credited to an absence of spiral density waves within the galaxy. However, Thornley (1996) presented K’ (2.1 $\mu$ m) observations of four nearby flocculent spiral galaxies<sup>1</sup> that clearly show low-level spiral structure, which suggests that kiloparsec-scale spiral structure is more prevalent in flocculent galaxies than previously thought. Interestingly, a comparison of the two PDLs with feathers seen in the HST WFPC2 image of NGC 5055 to the stellar spiral arm observed at 2.1 $\mu$ m shows that the feather PDLs and stellar arms are related structures (see Figure 18). This correlation between PDLs and spiral density waves suggests that feathers originating at delineated PDLs in flocculent galaxies may indicate an underlying spiral density wave not dominant at visible

---

<sup>1</sup>NGC 2403, NGC 3521, NGC 4414, NGC 5055

wavelengths.

As described in §4.2, flocculents also harbor extinction structures which appear morphologically nearly identical to classic feathers, which we called flocculent feathers; these differ in that they are *not* associated with PDLs and tend to be associated with less star formation per feature. They are nicely illustrated in NGC 7217 (Figure 14) as well as the parts of NGC 5055 (Figure 12) not associated with the PDLs. The number of flocculent feathers in a flocculent may greatly outnumber the classic feathers associated with PDLs. Flocculent feathers are likely due to gaseous/dusty condensations sheared by differential rotation. As mentioned previously, we detected flocculent feathers in 17 of 24 flocculent galaxies.

#### 4.4. A Catalog of Feather Morphology

General properties of the 45 galaxies with clearly delineated feathers are listed in Table 2. See Figures 5–14 for images of 21 of the 45 galaxies with classic feathers. We subjected this “catalog” of 45 galaxies to more detailed examination of feather morphology and characteristics.

##### 4.4.1. “Beads on a String”

As noted above, feathers are typically associated with star formation, particularly near where they emerge from the PDL and outer edge of a spiral arm. In 38 of the 45 galaxies with feathers, a series of bright OB associations and HII regions occur which fit the “beads on a string” description used by Piddington (1970) and Elmegreen (1980). The 38 galaxies with this characteristic are noted in Table 3. Typically, the star formation that comprises the “beads” is associated with feathers: near the beginning of feathers, along the PDL; lining feathers, within the arm; and in the interarm, as components of spurs. Spurs themselves are observed as short chains of star formation jutting outward from spiral arms at large angles. For example, along the outer edge of the spiral arms in NGC 3631 (Figure 9) several regions of OB associations are aligned in chains that are the beginnings of interarm spurs. Also present in the southern arm of NGC 3631 is a chain of OB associations along the PDL.

##### 4.4.2. *Evolution of Feathers to Spurs*

In eleven galaxies, we observe spurs on the outside of spiral arms, in the interarm regions, in addition to the star formation seen along feathers within arms. Within these

eleven galaxies (see Table 3) we find feathers that transition to spurs across the outer edge of the spiral arm (Figure 3), forming a composite feature. These feathers appear to evolve into spurs with star formation developing as gas flows downstream from the PDL. B88 and KO both predicted that spurs result from feathers. KO’s simulations follow the evolution of feathers through their fragmentation into self-gravitating clumps on the outer edge of a spiral arm. The observations are consistent with this picture.

#### 4.4.3. *Elongated Feathers*

As mentioned in §4.1, we also observe many feathers which are not solely contained within the luminous part of the spiral arms. These extend into the interarm similar to spurs; presumably these elongated feathers are the gaseous counterpart to spurs. Twenty-nine galaxies listed in Table 3 have elongated feathers, which are sometimes dotted with HII regions. Typically, elongated feathers are swept back more sharply in the interarm regions than they are at the outer edge of the luminous arm. The decrease in pitch angle along elongated feathers is due to the large interarm shear referred to in §4.4.5.

In many cases, elongated feathers merge into a common interarm dust lane. In 15 galaxies, the farthest reaching feathers actually merge with the PDL of the next arm.

#### 4.4.4. *Lattice Structure*

Another intriguing feather structure, present in 14 galaxies noted in Table 3, is a series of feathers that appear to link one or more pairs of PDLs, forming a lattice within a single spiral arm. An example of such a network of extinction features is in the northern arm of NGC 4579 (Figure 11) which includes several tiers of dust lanes connected by feathers emerging from the previous row. These multiple tracks should not be confused with the cases of elongated feathers that span an entire interarm region and merge with the PDL of another arm. Lattices are most common in strongly barred galaxies, and absent in unbarred galaxies. In total there are nine SB galaxies and five SAB galaxies with lattices in one or more arms. B88 predicted that multiple tracks of feathers could form if the background flow was sufficiently unstable, allowing growth along both preferred directions, parallel and perpendicular to the spiral arm.

#### 4.4.5. Shape of Feathers

The shape of a feather is a measure of the change in shear as gas passes through an arm. The pitch angles of feathers, as mentioned in §4.1, vary with the phase of an arm. Near the outer edges of an arm, feathers are almost always predominately trailing features. Well-delineated cases show, however, that they originate as leading features from the PDL, which marks the inner edge of a spiral arm.

The feathers described by B88, as well as those evident in the KO local MHD and DB hydrodynamical simulations, have the same characteristic shape as observed feathers. In these cases, both observations and models, the feathers emerge at a large, leading angle with respect to a spiral arm, and the pitch angles decrease outward. The outer portions of feathers are curved back into trailing features presumably by strong interarm shearing.

Nearest to the spiral arm, the feathers produced in the WK hydrodynamic simulations curve in the opposite sense to observed feathers (from trailing to leading). Further downstream in the interarm region, however, their features become trailing. This curvature is likely due to the rising background rotation curve they adopt.<sup>2</sup> Further, although the arm-interarm density ratio is  $\sim 100$ , their models do not include self-gravity. The WK model assumes physical conditions rather different from those where feathers have been observed: the gaseous disks are differentially rotating, self-gravity is important, and the arm-interarm surface density ratios are  $\approx 10$ . Thus the existing WK models are probably not relevant for observed feathers.

### 4.5. Feathers in the Spitzer $8\mu\text{m}$ Band

We have discussed feathers as extinction features. Despite the identification of some elongated feathers and also the association with spurs discussed in §4.4, extinction features

---

<sup>2</sup>If  $\Omega$  is the local angular velocity, local wavevectors rotate counterclockwise wherever

$$\frac{\partial \ln \Omega}{\partial \ln R} > 0$$

and clockwise where it is less than zero. Since

$$\frac{\partial \ln \Omega}{\partial \ln R} = \left( 1 + \frac{\partial \ln V_c}{\partial \ln R} \right) \frac{\Sigma}{\Sigma_o} - 2$$

where  $\Sigma$  is the local density and  $\Sigma_o$  is the mean density, a solid body rotation curve would imply trailing-to-leading curvature in any overdense ( $\Sigma > \Sigma_o$ ) region.

can be difficult to trace where the background stellar density is low or where there is confusing foreground or embedded emission. Recently released Spitzer SINGS data (Kennicutt et al. 2005) enable us to examine nine galaxies<sup>3</sup> from our catalog in the IRAC 3.6–8 $\mu$ m bands. These galaxies appear dramatically different at 8 $\mu$ m from their appearance at optical wavelengths. We observe that their 8 $\mu$ m spiral arms have prominent, bright features that extend well into the interarm, referred to as “filaments” in NGC 5194 by Calzetti et al. (2005). Particularly striking are NGC 5194 and NGC 0628 (see Figure 15 and Figure 16 for IRAC 8 $\mu$ m images).

The bright interarm features seen at 8 $\mu$ m emerge from the spiral arms at large pitch angles. Downstream from the arms, their pitch angle decreases with distance from the spiral arm. Some of the 8 $\mu$ m features span the entire interarm region and a few eventually merge with an outer arm, similarly to observed elongated feathers. The dark lines overlaid on the 8 $\mu$ m images in Figure 15 and Figure 16 represent the location and length of feathers as measured in the HST image of the corresponding galaxy. There appears to be a correlation between the elongated feathers observed in the visible and the bright interarm regions seen at 8 $\mu$ m.

The primary source of emission at 8 $\mu$ m is thought to be polycyclic aromatic hydrocarbons (PAHs), which are excited nonthermally by single UV photons (Sellgren 1984). PAHs are found in diffuse atomic clouds and in photodissociation-regions (PDRs) surrounding molecular clouds, where they are excited or photodissociated by stellar UV radiation (e.g. van Dishoeck 2004). Since the extinction that makes feathers visible is due to dust associated with relatively dense interstellar gas, it is not surprising that feathers should be traced by PAH emission at 8 $\mu$ m as we observe.

#### 4.6. Association of Feathers with Molecular Gas

As discussed in the previous section, 8 $\mu$ m emission can be used to trace feathers into the interarms, where extinction features are more difficult to observe. However, it is difficult to extract reliable gas column density estimates from either dust extinction or 8 $\mu$ m emission. Dust extinction depends on the unknown distribution of dust relative to illuminating stars. How are the stars distributed above and below the dust clouds? Is the dust layer homogeneous or clumped? What is the dust emissivity and the dust to gas ratio? Quantitative extraction of gas column density from 8 $\mu$ m emission has some of the same limitations, and also requires understanding of heating, formation, and destruction of PAHs. By contrast,

---

<sup>3</sup>NGC 0628, 1566, 4254, 4321, 4579, 4725, 4736, 5055, and 5194

interpretation of CO 1-0 emission is perhaps more straightforward, although it too has limitations. In this section, we evaluate the association of feathers with molecular gas emission as traced by CO 1-0 emission. Good observations are available for several galaxies from the BIMA SONG catalogue (Regan et al. 2001; Helfer et al. 2003).

In Figures 15 and 16 we show the locations of feathers (traced by lines) overlaid on maps of velocity-integrated CO 1-0 emission in NGC 0628 and NGC 5194. The figures show remarkable agreement between the location of CO peaks and the intersection of feathers with their PDL. Most feathers are very clearly associated with CO peaks and nearly all other feathers are plausibly associated with CO peaks. In fact, along the arms the correspondence is nearly one to one: nearly all CO peaks are associated with feathers. It should be noted that initially we drew the feather lines without reference to the CO maps and later noted the close association. For a few feathers, the precise location of the feather becomes unclear near the PDL owing to confusion from emission from massive star-forming regions. In these cases, we found that a straight-line extrapolation of the feather inward intersected the PDL slightly inward from the nearest CO peak; if instead we assumed a curvature similar to neighboring feathers, the line intersected the PDL close to the CO peak. For this small subset of feathers, we drew the line to have similar curvature and to intersect the CO peak.

The coincidence between CO peaks and the “base” of feathers is interesting, because it associates feathers with the highest gas surface density concentrations in the galaxy disk. It therefore connects the feather phenomenon with much of the star formation in the galaxy disk.

For some of the CO peaks, we see weak extensions in CO emission toward the outside of the arm along the feather. The dynamic range of the CO map is limited; nonetheless for the stronger CO peaks it is clear that the gas column density of feathers rapidly decreases by at least a factor of 5–10 with distance from the PDL. Thus, contrary to the impression given by both the dust extinction maps and the  $8\mu\text{m}$  Spitzer maps, CO maps show that the gas column density of feather features is by far the highest at the PDL. Although it is conceivable that the CO emissivity is higher in the arm, it is unlikely to vary by a factor of ten. The large enhancement in feather column density near the arm clearly pinpoints the PDL as the point of origin of the feather. Shear and divergent flow stretch out the condensations as the gas flows out of the arm. While the molecular gas is strongly peaked at the PDL, star formation (as traced by  $\text{H}\alpha$  and  $24\mu\text{m}$ ) tends to be more distributed along the feather *downstream* of the PDL.

#### 4.7. Feather Spacing and Gas Surface Density

It is clear from inspection of the HST images that the spacing between feathers tends to increase with galactocentric radius, as can be seen for example in Figures 15 and 16. This might be related to the gas surface density, which generally decreases with distance from the nucleus, and so it is interesting to compare feather spacings with gas column density. We made this comparison for two galaxies with both extensive feathers and good CO maps, NGC 0628 and NGC 5194. For this comparison we used the BIMA SONG CO 1-0 velocity-integrated maps, and sampled the CO maps along the PDLs of each spiral arm at  $3''$  spacings (half beam width). We then estimated the  $H_2$  column densities using the relation

$$N_{H_2} = 2.2 \times 10^{20} \left( \frac{I_{CO}}{\text{K km s}^{-1}} \right) \text{ cm}^{-2},$$

(Strong et al. 1988). The corresponding molecular surface density at each point is then

$$\Sigma_{H_2} = 2.17 \times 10^{-20} N_{H_2} \cos i \ M_{\odot} \text{ pc}^{-2}.$$

Noting that the gas surface densities are significantly lower in NGC 0628 than NGC 5194, we included azimuthally averaged HI data (Shostak & van der Kruit 1984) to obtain a lower limit on the total gas surface density. The radial atomic surface density is

$$\Sigma_{H_I} = 1.08 \times 10^{-20} N_{H_I} \cos i \ M_{\odot} \text{ pc}^{-2}$$

and the *total* gas surface density is  $\Sigma_{\text{gas}} = \Sigma_{H_2} + \Sigma_{H_I} \ M_{\odot} \text{ pc}^{-2}$ .

We plot (see Figures 19 and 20) the gas surface density versus the *deprojected* distance along the arms in both galaxies using the HST ACS image of NGC 5194 (larger FOV than WFPC2) and the HST WFPC2 image of NGC 0628. Also shown at the bottom of each figure are ticks marking the location of feathers along the arms.

In NGC 5194, the surface density rises from the beginning of both arms, peaking near a galactocentric radius of 1 kpc. Thereafter, the surface density generally declines, although there are significant fluctuations. Note that in the inner 1–2 kpc the peaks in Arm 1 tend to be higher (sometimes by a factor of two), but at larger radii Arm 2 peaks sometimes have higher surface density. Overall, it can be seen that the spacing between feathers increases as the surface density decreases along each arm, and that the feathers generally coincide with the gas column density peaks.

NGC 0628 also exhibits a general decline in surface density with radius although there are significant peaks at larger radii. As in NGC 5194, generally feather spacing increases



and gas column density decreases as one moves out along the arm. However, the gas surface densities are lower by at least a factor of three compared to NGC 5194; the peak surface density in NGC 5194 is at least an order of magnitude higher.

The increase in feather spacing with decreasing gas surface density along a spiral arm and the association of feathers and gas surface density peaks evident in Figures 19 and 20 suggest a gravitational instability, such as the Jeans instability. To investigate this further, we estimated the Jeans length as

$$\lambda_{Jeans} = c_s^2 / (G\Sigma),$$

where  $c_s$  is the effective sound speed. We adopt  $c_s = 7 \text{ km s}^{-1}$  for both NGC 0628 and NGC 5194.

Figure 21 shows the feather separations and Jeans lengths, along with their ratio as a function of distance along each arm in NGC 5194. Figure 22 shows the same quantities for NGC 0628. Noticing that feathers tend to “clump” together in groups, with larger distances separating the groups than the average distance between the feathers within a group, we averaged the separations, Jeans length, and ratios separately for each group. For NGC 5194, it can be seen that the feather spacing increases from  $\sim 200$  pc in the inner galaxy to 500–1000 pc in the outer galaxy. Since the Jeans length increases by a similar factor, the ratio of separation to Jeans length does not exhibit a radial trend. NGC 0628 also shows evidence for some increase in feather spacing with galactocentric radius, while the ratio of separation to Jeans length is relatively flat.

While the feather spacings in NGC 0628 and NGC 5194 are roughly similar, the measured ratio of feather spacing to Jeans length is a factor of 4–6 higher in NGC 5194 and differs between its arms. The lower ratios in NGC 0628 are probably due in part to the greater fraction of gas in NGC 0628 likely being in atomic form. Although we have included azimuthally averaged HI (Shostak & van der Kruit 1984) to calculate the total gas surface density, the HI data are at low resolution ( $13.8'' \times 48.5''$ ), and therefore the column densities are lower limits. In NGC 5194, the addition of HI is not a problem since the gas is overwhelmingly molecular, but in NGC 0628 the unresolved HI column density could be substantial. Another factor lowering the measured ratio is that a significant fraction of the CO flux is likely undetected in NGC 0628, owing to low signal to noise (Helfer et al. 2002, 2003). Thus, while the peaks and radial trends observed for NGC 0628 are credible, the magnitudes of the Jeans length and ratio are probably only useful for NGC 5194.

We also measured the separation of feathers in NGC 3433 and NGC 5985, Figure 8 and Figure 12. As in NGC 0628 and NGC 5194, both galaxies display a trend of increasing

separation along an arm. In NGC 3433, the average separation along Arm 1 is 310 pc between 0.9 kpc and 2.9 kpc galactocentric radius. For Arm 2, the average is 380 pc between 1.5 kpc and 1.6 kpc and 430 pc between 2.7 kpc and 7.1 kpc. In NGC 5985, the average separation along Arm 1 is 445 pc between 3.7 kpc and 5.1 kpc. For Arm 2, the average is 770 pc between 3.0 kpc and 3.1 kpc.

It would of course be interesting to measure and characterize the typical feather spacing in more galaxies. However, either due to the quality of observations, the complexity of extinction substructure, or the contamination due to star formation, most of the images did not lend themselves to reliable estimates of feather spacings. As we have shown, molecular gas offers a non-extincted, less-confused tracer of feathers. Therefore, separation measurements using CO observations with CARMA and ALMA may yield better estimates in more galaxies.

Feather spacings found in NGC 0628 and NGC 5194 are typically larger than the 100–200 pc range predicted by WK. DB predicted feather spacings of 700 pc; such large spacings are only seen in the outer part of Arm 2 in NGC 5194. We note that DB and WK did not include self-gravity in their calculation; particularly in NGC 5194, the observed gas densities are comparable or larger the stellar surface densities, indicating that self-gravity is likely important.

KO and Kim & Ostriker 2006 predicted the characteristic spacing of feathers to be up to 7–10 times the local Jeans length for their magnetized models, which are stable to quasi-axisymmetric modes. For models which are unstable to quasi-axisymmetric modes, the arms do not have a well-defined “pre-fragmentation” surface density, but the feather spacings are in general smaller. The range in ratios of feather spacing to Jeans length observed in NGC 5194 centers on the values of 7–10 predicted by KO. This, along with the increase in feather spacing with decreasing gas surface density and the correlation between the location of feathers and gas surface density peaks, is consistent with the view that feathers form via a gravitational instability.

## 5. Conclusions

We find extinction feathers in nearly 20% of 233 spiral galaxies. We show that feathers are most common in Sb–Sc galaxies; Sb–Sc galaxies in which we did not detect feathers either had poor quality images, or flocculent or complex structure. Feathers are rare in Sa galaxies and undetected in Scd–Sd galaxies. The presence of feathers is closely tied to the existence of a primary dust lane (PDL). The probability of detecting feathers increases with PDL delineation; the highest being 83% for spirals with well-delineated PDLs, within

which feathers are ubiquitous. Characteristically, feathers: (1) are associated with bright star forming regions within spiral arms and interarm regions; (2) extend beyond the outer edge of spiral arms, sometimes far into interarm regions, and merging with the PDL of another arm; (3) transition or evolve into stellar spurs; and (4) often form lattice structures or multiple rows of feathers within a single spiral arm in barred galaxies. Furthermore, we find that the spacing of feathers is related to the molecular surface density along spiral arms; (1) typically, the distance between feathers increases as the molecular surface density decreases and (2) the majority of feathers originate in regions of higher gas surface density. The mean separation of feathers is  $1.7\lambda_{Jeans}$  and  $10.4\lambda_{Jeans}$  in NGC 0628 and NGC 5194; the value for NGC 0628 is likely an underestimate due to poor signal to noise and a lower limit of HI data. The above observable characteristics are consistent with models in which feathers are produced by local gravitational instabilities (i.e. Jeans or magneto-Jeans instability) in the gas.

## 6. Acknowledgments

This research is supported in part by grants AST-0228974 and AST-0507315 from the National Science Foundation. We made use of the NASA/IPAC Extragalactic Database (NED) which is operated by the Jet Propulsion Laboratory, California Institute of Technology, under contract with the National Aeronautics and Space Administration. This work is based in part on observations made with the Spitzer Space Telescope, which is operated by the Jet Propulsion Laboratory, California Institute of Technology under NASA contract 1407.

## REFERENCES

- Balbus, S. A. 1988, *ApJ*, 324, 60 (B88)
- Beckwith, S., NASA, ESA, and The Hubble Heritage Team (STScI/AURA) 2005, Hubble Heritage image of M51 (Baltimore, STScI), <http://heritage.stsci.edu/2005/12a/index.html>
- Calzetti, D., et al. 2005, *ApJ*, 633, 871
- Chakrabarti, S., Laughlin, G., & Shu, F. H. 2003, *ApJ*, 596, 220 (CLS)
- de Vaucouleurs, G., de Vaucouleurs, A., Corwin, H. G., Buta, R. J., Paturel, G., & Fouque, P. 1995, *VizieR Online Data Catalog*, 7155, 0
- Dobbs, C. L., & Bonnell, I. A. 2006, *ArXiv Astrophysics e-prints*, arXiv:astro-ph/0602100

- Elmegreen, D. M. 1980, *ApJ*, 242, 528
- Elmegreen, D. M. & Elmegreen, B. G. 1987, *ApJ*, 314, 3
- Elmegreen, D. M., Elmegreen, B. G., Frogel, J. A., Eskridge, P. B., Pogge, R. W., Gallagher, A., & Iams, J. 2002, *AJ*, 124, 777
- Helfer, T. T., Vogel, S. N., Lugten, J. B., & Teuben, P. J. 2002, *PASP*, 114, 350
- Helfer, T. T., Thornley, M. D., Regan, M. W., Wong, T., Sheth, K., Vogel, S. N., Blitz, L., & Bock, D. C.-J. 2003, *ApJS*, 145, 259
- Kennicutt, R. C., et al. 2005, Delivery of Data from the Spitzer Legacy Project: IRAC, IRS, & MIPS (Pasadena, SSC), <http://ssc.spitzer.caltech.edu/legacy/original.html>
- Kim, W. & Ostriker, E. C. 2002, *ApJ*, 570, 132 (KO)
- Kim, W.-T., & Ostriker, E. C. 2006, ArXiv Astrophysics e-prints, arXiv:astro-ph/0603751
- Larsen, S. S., & Richtler, T. 1999, *A&A*, 345, 59
- Lynds, B. T. 1970, in *IAU Symp. 38, The Spiral Structure of Our Galaxy*, ed. W. Becker & G. Contopoulos (Dordrecht:Reidel), 26
- Piddington, J. H. 1973, *ApJ*, 179, 755
- Regan, M. W., Thornley, M. D., Helfer, T. T., Sheth, K., Wong, T., Vogel, S. N., Blitz, L., & Bock, D. C.-J. 2001, *ApJ*, 561, 218
- Sandage, A. 1961, Washington: Carnegie Institution, 1961
- Scoville, N. Z., Polletta, M., Ewald, S., Stolovy, S. R., Thompson, R., & Rieke, M. 2001, *AJ*, 122, 3017
- Sellgren, K. 1984, *ApJ*, 277, 623
- Shostak, G. S., & van der Kruit, P. C. 1984, *A&A*, 132, 20
- Strong, A. W., et al. 1988, *A&A*, 207, 1
- Thornley, M. D. 1996, *ApJL*, 469, L45
- van der Kruit, P. C. & de Bruyn, A. G. 1976, *A&A*, 48, 373
- van Dishoeck, E. F. 2004, *ARA&A*, 42, 119
- Wada, K. & Koda, J. 2004, *MNRAS*, 349, 270 (WK)
- Weaver, H. 1970, in *IAU Symp. 39, Interstellar Gas Dynamics*, ed. H Habing (Dordrecht: Kluwer), 22

Table 1. Delineation of Primary Dust Lanes and Frequency of Feather Detection

Primary Dust Lane Delineation	# of Galaxies	# of Galaxies with Feathers	% with Feathers
Poor	142	4	3%
Fair	46	12	26%
Good	35	29	83%
Total	223	45	20%

Table 2. Properties of the 45 Galaxies with Clearly Delineated Feathers

Galaxy	Figure Number	Type	Incl. (deg)	PA (deg)	$B_T$ (mag)	CZ ( $\text{km s}^{-1}$ )	Arm Class (EE)
IC 2056		RSABRbc*	34	8	12.48	1099	
NGC 0214	5	SABRbc	42	35	12.86	4495	9
NGC 0289		SBTbc	45	130	11.72	1690	12
NGC 0488		SARb	42	15	11.15	2233	3
NGC 0613		SBTbc	41	120	10.73	1510	9
NGC 0628	2, 4	SASc	24	25	10.01	632	9
NGC 0986		SBTab	41	150	11.64	1994	
NGC 1241	5	SBTb	53	140	12.64	3939	4
NGC 1300	6	SBTbc	49	106	11.11	1592	12
NGC 1365	5	SBSb	57	32	10.23	1675	12
NGC 1512		SBRa	51	90	11.13	735	6
NGC 1566	7	SABSbc	37	60	10.13	1449	12
NGC 1667		SABRc	39		12.77	4587	
NGC 2207		SABTbcP	50	141		2728	5
NGC 2336	7	SABRbc	57	178	11.26	2205	9
NGC 2339	8	SABTbc	41	175	11.98	2361	5
NGC 2997		SABTc	41	110	10.06	1090	9
NGC 3177	8	SATb	36	135	12.9	1220	6
NGC 3433	8	SASc	27	50	12.29	2591	9
NGC 3631	9	SASc	17		11.05	1143	9
NGC 3783		PSBRab	27			2926	9
NGC 4030		SASbc	44	27		1449	9
NGC 4254	9	SASc	29		10.17	2453	9
NGC 4303		SABTbc	27		10.18	1607	9
NGC 4321	10	SABSbc	32	30	10.26	1579	12
NGC 4394		RSBRb	27		11.73	772	6
NGC 4548	10	SBTb	37	150	11.04	498	5
NGC 4579	11	SABTb	37	95	10.68	1627	9
NGC 4593		RSBTb	42			2662	5
NGC 4647		SABTc	37	125	11.94	1421	3
NGC 4725		SABRabP	45	35	10.11	1180	6
NGC 4736	11	RSARab	36	105	8.99	297	3
NGC 5055	12	SATbc	55	105	9.57	516	3
NGC 5194	1, 3	SASbcP	24	170	9.08	463	12
NGC 5236	13	SABSbc	27		8.31	503	9
NGC 5248		SABTbc	44	110	10.97	1189	12

Table 2—Continued

Galaxy	Figure Number	Type	Incl. (deg)	PA (deg)	$B_T$ (mag)	CZ (km s <sup>-1</sup> )	Arm Class (EE)
NGC 5383		PSBTb*P	32	85	12.05	2226	12
NGC 5427		SAScP	32		11.93	2645	9
NGC 5643		SABTc	29		10.74	1163	
NGC 5970		SBRc	48	88	12.24	2063	9
NGC 5985	12	SABRb	58	13	11.67	2467	9
NGC 6753		RSARb	29	30	11.97	3142	8
NGC 6814		SABTbc	21		12.06	1509	9
NGC 6890	14	SATb	37	152	13.05	2471	
NGC 7392		SASbc	54	123	12.62	2908	5

Table 3. Feather Characteristics

Galaxy	Figure Number	Feather <sup>a</sup> ⇒ Spur	“Beads on a String”	Elongated Feathers	Lattice of Feathers
IC 2056			x		x
NGC 0214	5		x	x	
NGC 0289				x	x
NGC 0488				x	
NGC 0613			x		
NGC 0628	2, 4		x	x	
NGC 0986		x	x	x	x
NGC 1241	5		x		
NGC 1300	6	x	x	x	x
NGC 1365	5		x		x
NGC 1512			x	x	x
NGC 1566	7	x	x	x	
NGC 1667			x	x	
NGC 2207			x		
NGC 2336	7		x	x	
NGC 2339	8				
NGC 2997			x		
NGC 3177	8		x	x	
NGC 3433	8	x	x	x	
NGC 3631	9	x	x	x	
NGC 3783			x	x	
NGC 4030			x		
NGC 4254	9		x	x	
NGC 4303			x		
NGC 4321	10		x		
NGC 4394				x	x
NGC 4548	10		x	x	x
NGC 4579	11			x	x
NGC 4593			x		x
NGC 4647			x	x	
NGC 4725		x	x	x	
NGC 4736	11		x	x	
NGC 5055	12				
NGC 5194	1, 3	x	x	x	
NGC 5236	13	x	x	x	x
NGC 5248			x		



Table 3—Continued

Galaxy	Figure Number	Feather <sup>a</sup> ⇒ Spur	“Beads on a String”	Elongated Feathers	Lattice of Feathers
NGC 5383			x		x
NGC 5427		x	x	x	
NGC 5643			x		x
NGC 5970			x	x	
NGC 5985	12	x	x	x	x
NGC 6753			x	x	
NGC 6814				x	
NGC 6890	14		x		
NGC 7392			x	x	

<sup>a</sup>Galaxies within which we identified feathers transitioning into spurs.

Fig. 1.— A prototypical galaxy with feathers, NGC 5194. Feathers are marked by white lines.

Fig. 2.— A prototypical galaxy with feathers, NGC 0628. Feathers are marked by white lines.

Fig. 3.— NGC 5194, with the feather overlay omitted.

Fig. 4.— NGC 0628, with the feather overlay omitted.

Fig. 5.— *Top left:* NGC 0214, *Top right:* NGC 1241, *Bottom:* NGC 1365. The white arrows mark identified feathers.

Fig. 6.— Image: NGC 1300. The white arrows mark identified feathers.

Fig. 7.— *Top*: NGC 1566, *Bottom*: NGC 2336. The white arrows mark identified feathers.



Fig. 8.— *Top left:* NGC 2339, *Top right:* NGC 3177, *Bottom:* NGC 3433. The white arrows mark identified feathers.

Fig. 9.— *Top*: NGC 4254, *Bottom*: NGC 3631. The white arrows mark identified feathers.

Fig. 10.— *Top*: NGC 4321, *Bottom*: NGC 4548. The white arrows mark identified feathers.

Fig. 11.— *Top*: NGC 4579, *Bottom*: NGC 4736. The white arrows mark identified feathers.

Fig. 12.— *Top*: NGC 5055, *Bottom*: NGC 5985. The white arrows mark identified feathers.

Fig. 13.— Image: NGC 5236 (Larsen and Richtler 1999). The white arrows mark identified feathers.

Fig. 14.— *Top*: NGC 6890, the white arrows mark identified feathers. *Bottom*: NGC 7217, an example of a galaxy with flocculent feathers.

Fig. 15.— Two views of NGC 5194, with lines marking the feathers from HST image shown in Fig. 1 –  
*Top*: Spitzer  $8\mu\text{m}$  image. *Bottom*: BIMA SONG CO(J=1-0) image.



Fig. 16.— Two views of NGC 0628, with lines marking the feathers from HST image shown in Fig. 2 –  
*Top*: Spitzer  $8\mu\text{m}$  image. *Bottom*: BIMA SONG CO(J=1-0).

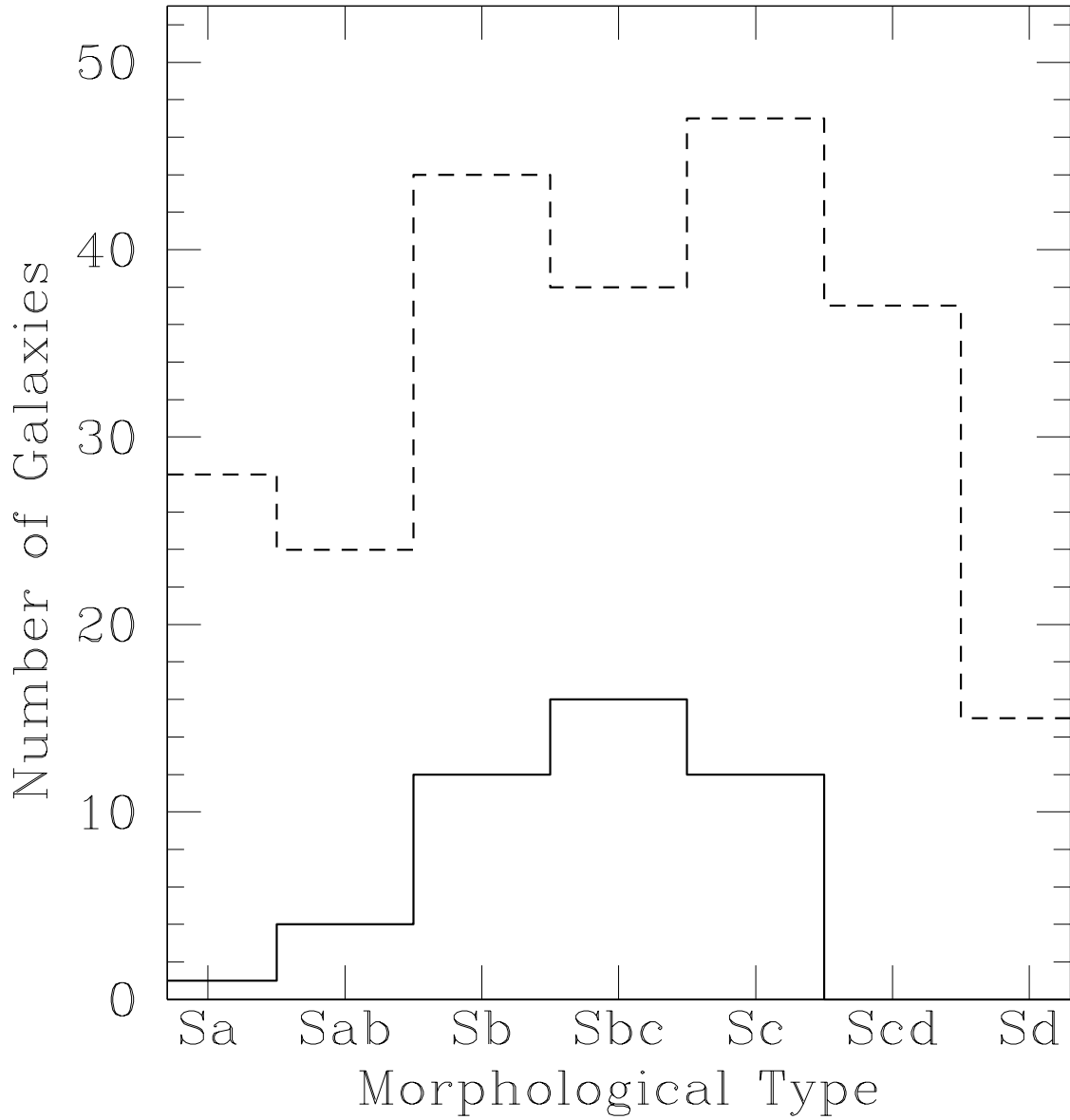


Fig. 17.— Distribution of galactic morphological types included in sample. The dashed line represents the distribution of morphological types of all the galaxies in the sample. The solid line shows the distribution for galaxies with feathers.

Fig. 18.— *Top*: WFPC2 HST F814W band image of NGC 5055. *Bottom*:  $2.1\mu\text{m}$  image. The thin grey lines in the HST image indicate observed PDLs within the galaxy. The same lines are overlaid on the  $2.1\mu\text{m}$  image, which show there is a clear association between PDLs observed in the visible and observed infrared emission marking the peak of the stellar arms.

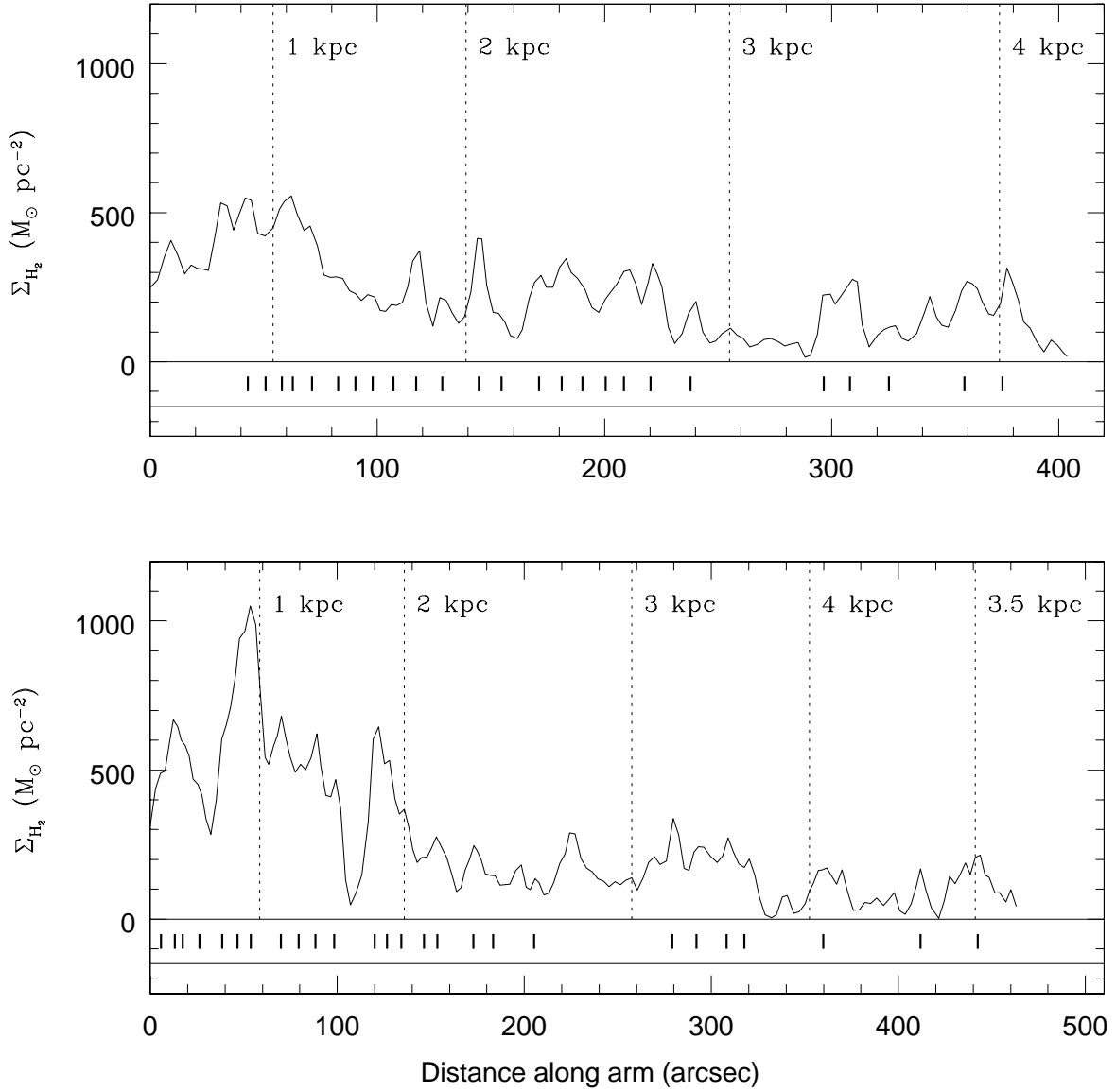


Fig. 19.— Variation in surface density along Arm 1 (top) and Arm 2 (bottom) in NGC 5194. The short vertical lines indicate the location of a feather along an arm. The dotted vertical lines indicate galactocentric radius. Note that Arm 2 bends inward near  $\sim 4$  kpc.

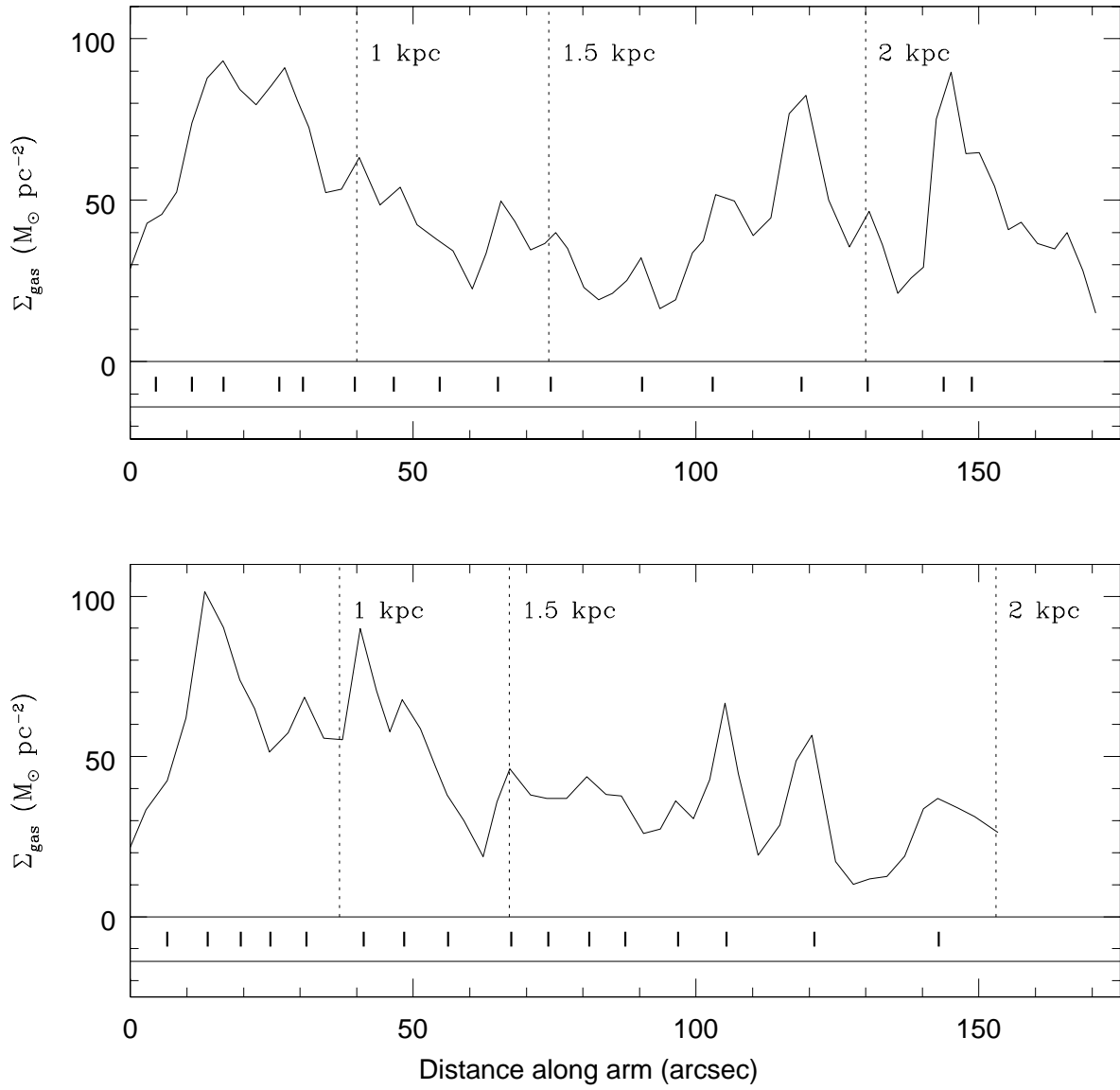


Fig. 20.— The same as Figure 19, for NGC 0628.

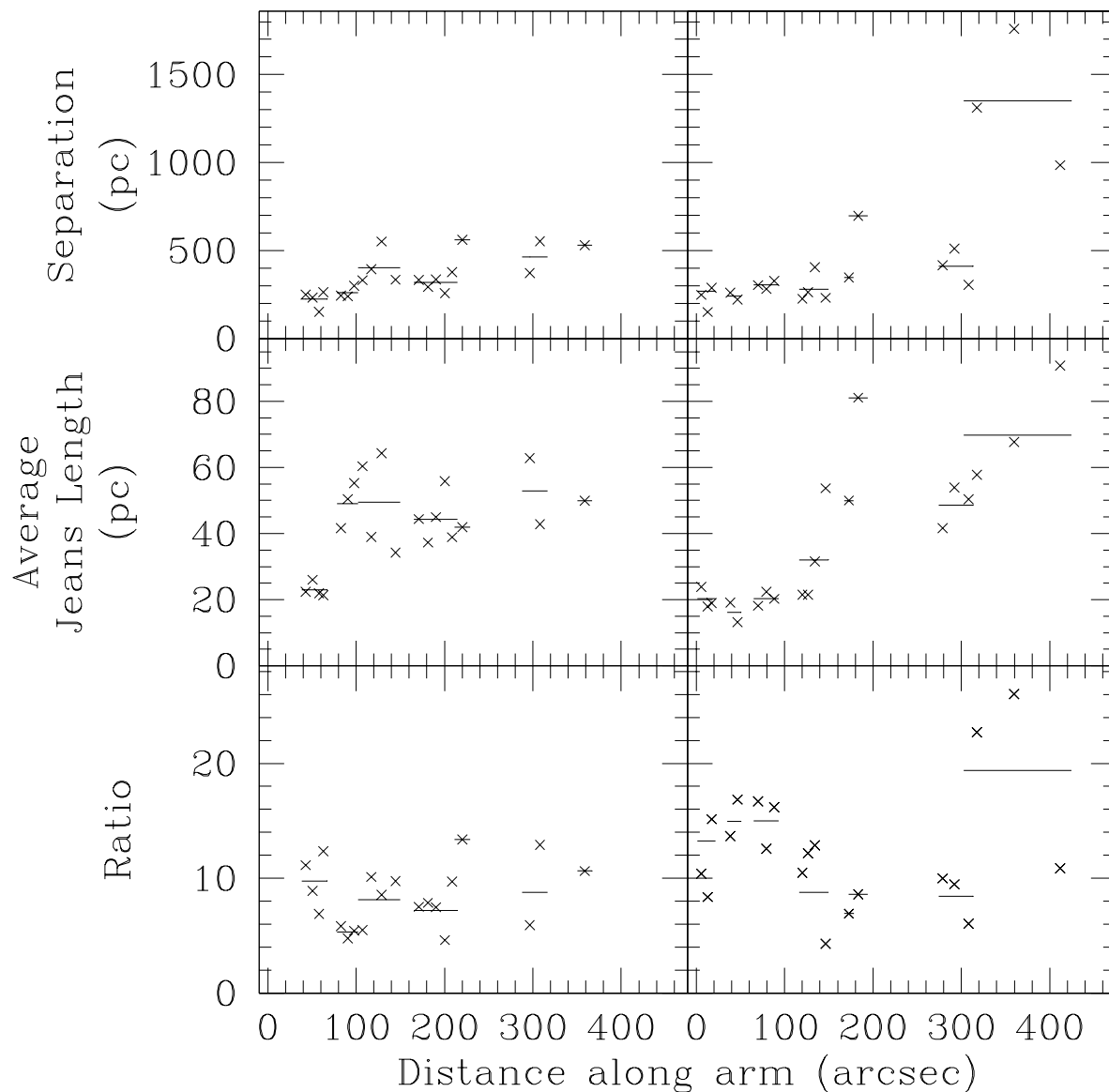


Fig. 21.— Comparison of feather separation to the local Jeans length averaged over  $6''$  in NGC 5194, as a function of distance along an arm; the left and right columns show data for Arms 1 and 2, respectively. (*Top*) Deprojected feather separation. (*Middle*) Average Jeans length at each feather. (*Bottom*) Ratio of deprojected feather spacing to the local Jeans length. The lines indicate the mean value for each group of feathers along an arm; the length of a line indicates the width of a group.

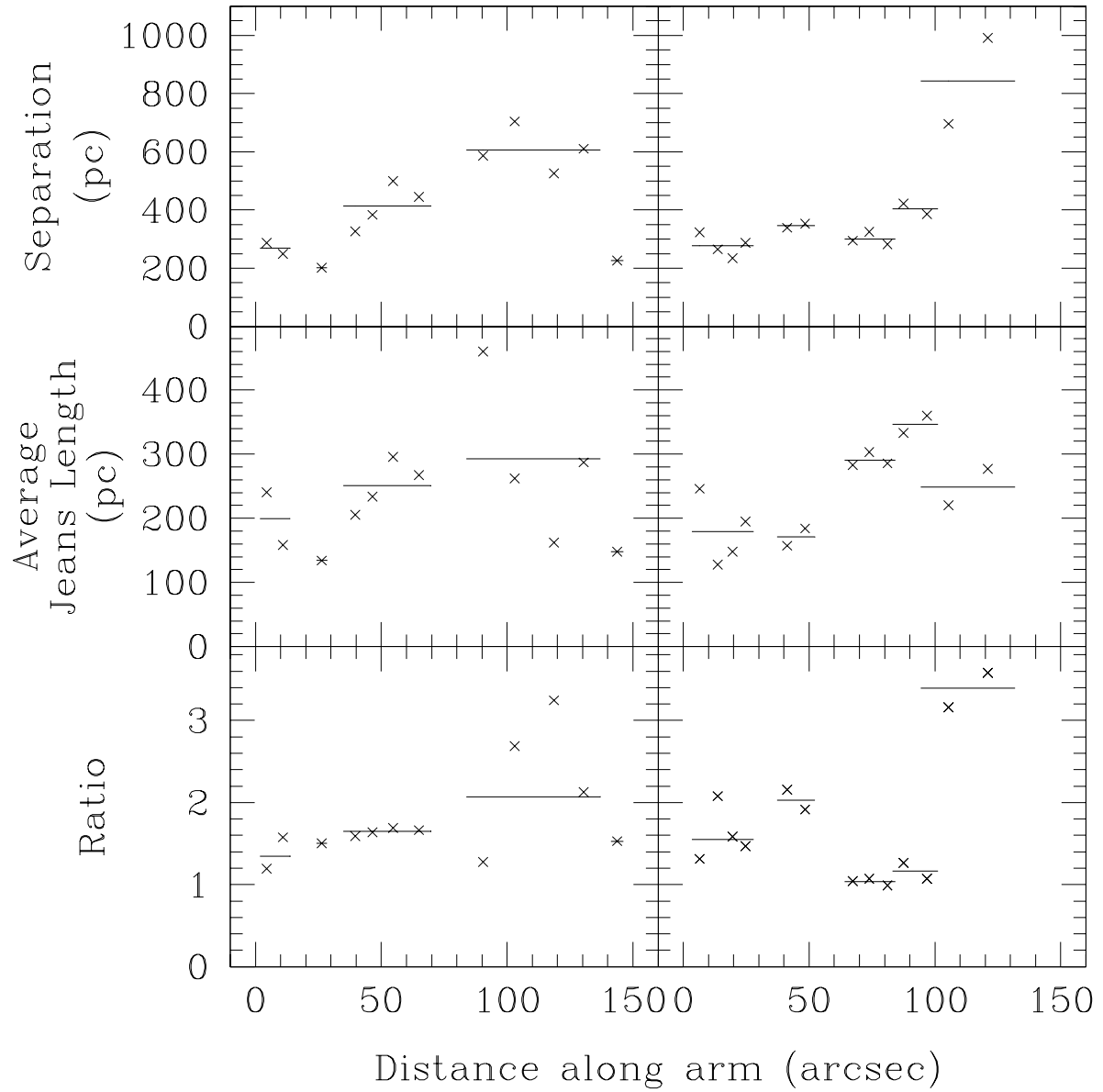


Fig. 22.— The same as Figure 21, for NGC 0628.

This figure "f1.jpg" is available in "jpg" format from:

<http://arxiv.org/ps/astro-ph/0606761v1>



This figure "f2.jpg" is available in "jpg" format from:

<http://arxiv.org/ps/astro-ph/0606761v1>

This figure "f3.jpg" is available in "jpg" format from:

<http://arxiv.org/ps/astro-ph/0606761v1>

This figure "f4.jpg" is available in "jpg" format from:

<http://arxiv.org/ps/astro-ph/0606761v1>

This figure "f5.jpg" is available in "jpg" format from:

<http://arxiv.org/ps/astro-ph/0606761v1>

This figure "f6.jpg" is available in "jpg" format from:

<http://arxiv.org/ps/astro-ph/0606761v1>

This figure "f7.jpg" is available in "jpg" format from:

<http://arxiv.org/ps/astro-ph/0606761v1>

This figure "f8.jpg" is available in "jpg" format from:

<http://arxiv.org/ps/astro-ph/0606761v1>

This figure "f9.jpg" is available in "jpg" format from:

<http://arxiv.org/ps/astro-ph/0606761v1>



This figure "f10.jpg" is available in "jpg" format from:

<http://arxiv.org/ps/astro-ph/0606761v1>

This figure "f11.jpg" is available in "jpg" format from:

<http://arxiv.org/ps/astro-ph/0606761v1>

This figure "f12.jpg" is available in "jpg" format from:

<http://arxiv.org/ps/astro-ph/0606761v1>

This figure "f13.jpg" is available in "jpg" format from:

<http://arxiv.org/ps/astro-ph/0606761v1>

This figure "f14.jpg" is available in "jpg" format from:

<http://arxiv.org/ps/astro-ph/0606761v1>

This figure "f15.jpg" is available in "jpg" format from:

<http://arxiv.org/ps/astro-ph/0606761v1>

This figure "f16.jpg" is available in "jpg" format from:

<http://arxiv.org/ps/astro-ph/0606761v1>

This figure "f18.jpg" is available in "jpg" format from:

<http://arxiv.org/ps/astro-ph/0606761v1>